Delta-Normids (DNO#915) outburst in 2026

Paul Roggemans[1], **Denis Vida**[2,3], **Damir Šegon**[4,5], **James M. Scott**[6], **Jeff Wood**[7]

[1] **Pijnboomstraat 25, 2800 Mechelen, Belgium**
Paul.roggemans@gmail.com

[2] **Department of Physics and Astronomy, University of Western Ontario, Richmond Street, London, N6A 3K7, Ontario, Canada**

[3] **Institute for Earth and Space Exploration, University of Western Ontario, Perth Drive, London, N6A 5B8, Ontario, Canada**
denis.vida@gmail.com

[4] **Astronomical Society Istra Pula, Park Monte Zaro 2, 52100 Pula, Croatia**

[5] **Višnjan Observatory, Istarska 5, 52463 Višnjan, Croatia**

[6] **Department of Geoscience, Aarhus University, Høegh-Guldbergs Gade 2. DK-8000 Aarhus C, Denmark**

[7] **PO Box 162, Willetton, Western Australia 6955, Australia**

A sharp short-duration outburst was recorded during 22–23 February, 2026 from a radiant at R.A. = 238.5° and Decl.= –46.0°, with a geocentric velocity of 66.7 km/s. The shower is identified as the delta-Normids, and Comet C/1861 Y1 (Tuttle) could be the parent body. This case study confirms the existence of this annual meteor shower that fulfils the criteria for it to be nominated as having an established status by the IAU-MDC.

1 Introduction

Between 22–23 February, 2026, a bright spot revealed a strong outburst of a minor shower on the GMN radiant density maps (*Figure 1*). The activity was identified as the delta-Normids (DNO-915)[21] and the outburst reported to the astronomical community (Vida et al., 2026). A more in-depth case study was made based upon GMN orbit data collected for this shower since 2020.

The delta-Normids were discovered by CAMS (Jenniskens, 2023). A possible connection with the gamma-Normids (GMO-118) is unlikely since this shower appears later in time according to visual observers.

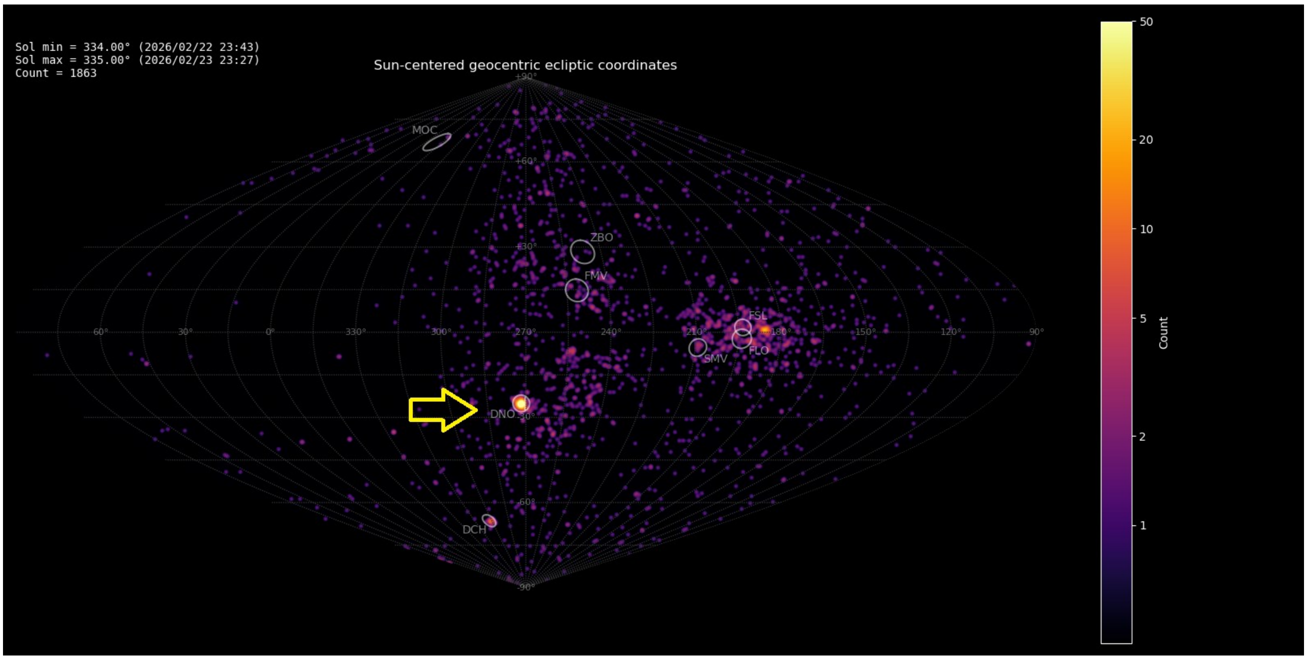

Figure 1 – Radiant density map with 1863 radiants obtained by the Global Meteor Network during 22–23 February, 2026. The position of the delta-Normids in Sun-centered geocentric ecliptic coordinates is marked with a yellow arrow.

[21] https://www.ta3.sk/IAUC22DB/MDC2022/Roje/pojedynczy_obiekt.php?lporz=02243&kodstrumienia=00915

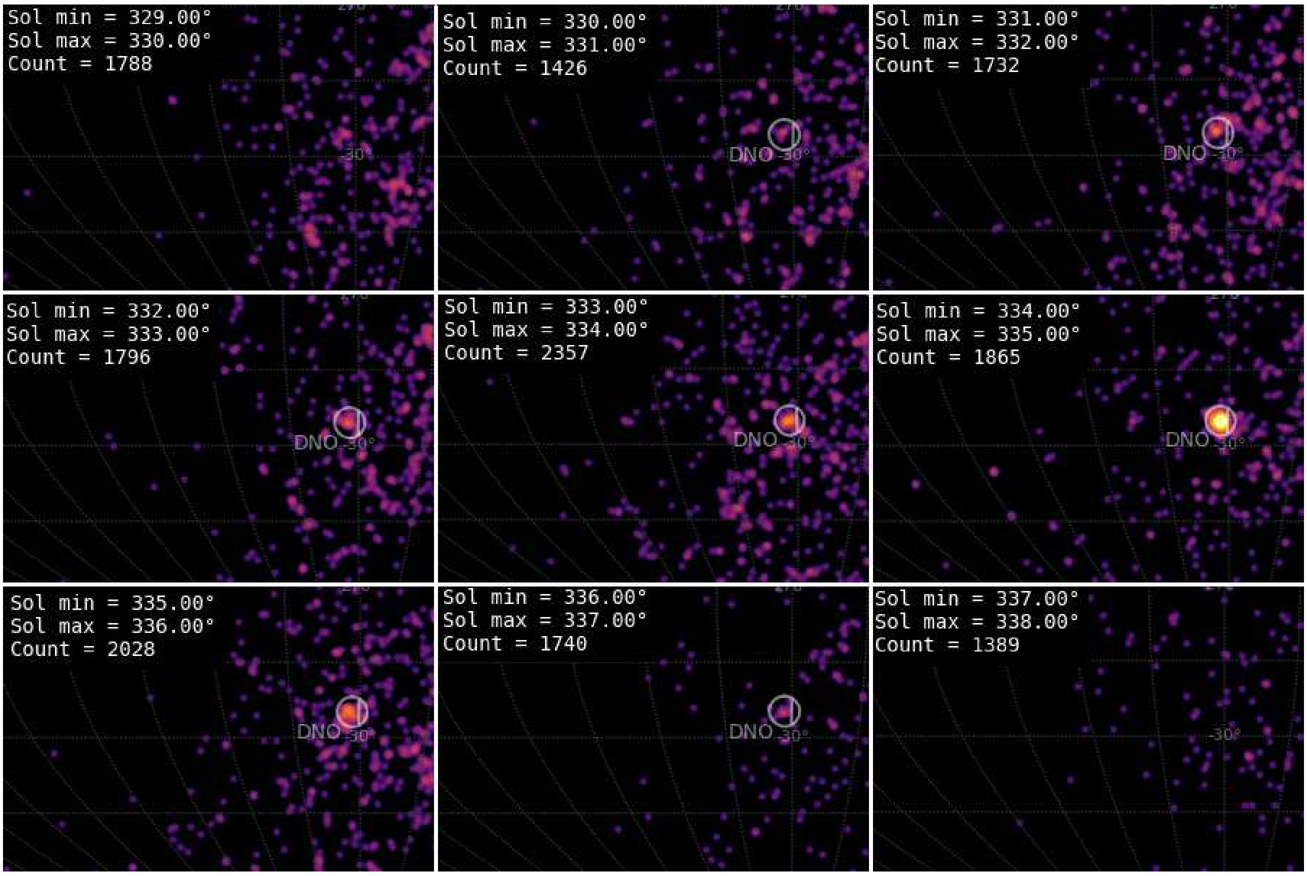

Figure 2 – The appearance of the delta-Normids during consecutive nights, the outburst appeared at $\lambda_{\odot} = 334.7°$.

2 Shower classification based on radiants

The GMN shower association criteria assume that meteors within 1° in solar longitude, within 1.4° of a common radiant, and within 10% in geocentric velocity of a shower reference location are members of that shower. Further details about the shower association are explained in Moorhead et al. (2020). Using these meteor shower selection criteria, 281 orbits have been identified as delta-Normids recorded in 2026 by 213 GMN cameras installed in Australia, Brazil, New Zealand, South-Korea, United States and South Africa. The final results have been listed in *Table 2*.

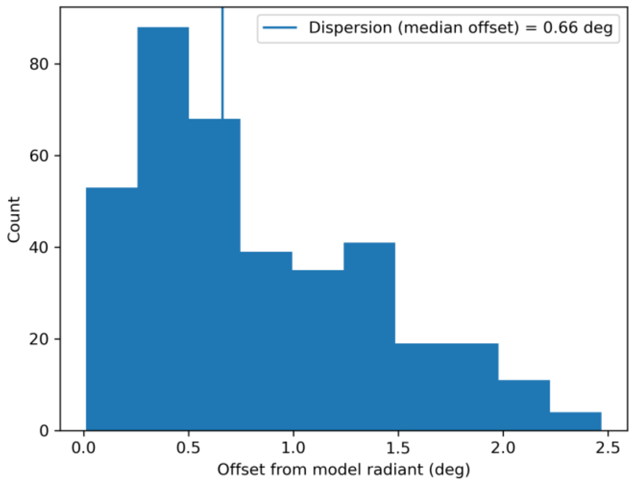

Figure 3 – Dispersion median offset on the radiant position.

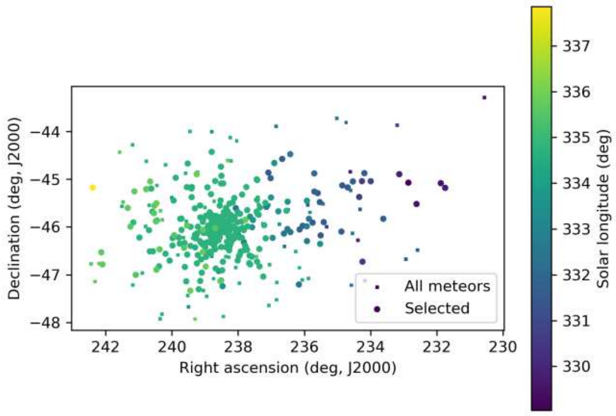

Figure 4 – The radiant distribution during the solar-longitude interval 329° – 338° in equatorial coordinates.

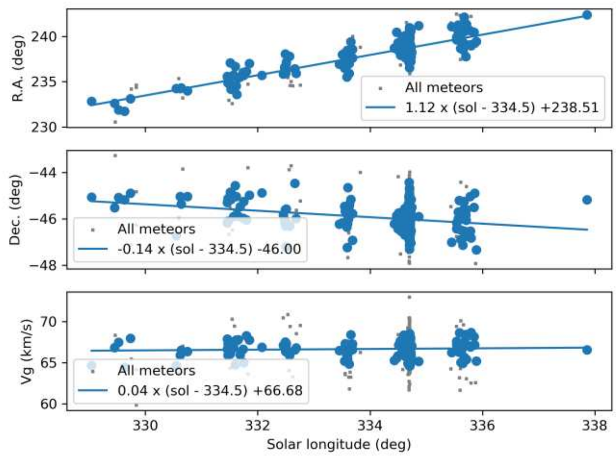

Figure 5 – The radiant drift.

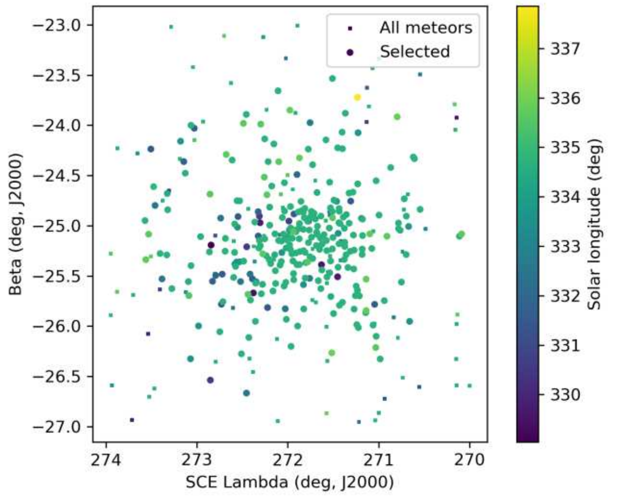

Figure 6 – The radiant distribution during the solar-longitude interval 329° – 338° in Sun centered geocentric ecliptic coordinates.

3 Shower classification based on orbits

A complete independent meteoroid stream search has been applied to orbit data obtained between solar longitude 320.0° and 360.0° during the years 2019 to 2026. 249194 orbits were available within this time interval and a final mean orbit has been computed by the method of Jopek et al. (2006) for the thresholds according to the Rayleigh fit in *Figure 7*, $D_{SH} < 0.125$ and $D_D < 0.05$ and $D_J < 0.125$ (Southworth and Hawkins, 1963; Drummond, 1981; Jopek, 1993. The results and mean orbit based upon 437 meteors for 2020–2026 are listed in *Table 2*. The method has been described in detail in a separate publication (Roggemans et al., 2026a).

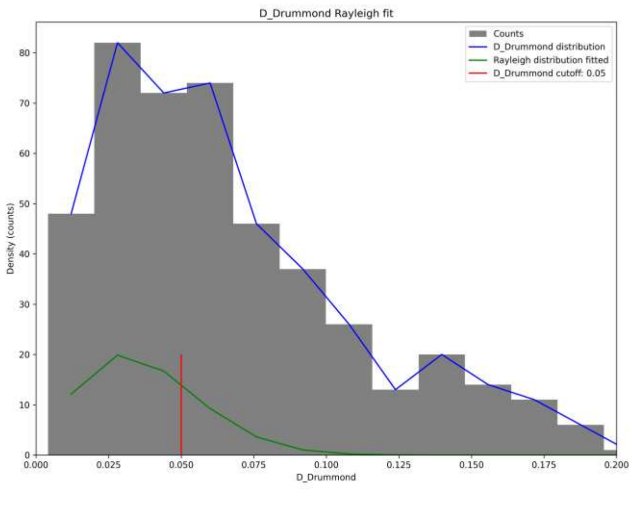

Figure 7 – Rayleigh fit on the Drummond criterion for delta-Normids, 2026 data.

Both methods identified 332 delta-Normids in 2026, 190 (57.2%) in common. The radiant classification method counted 92 (27.7%) delta-Normids that failed to fit the orbit thresholds with $D_{SH} < 0.125$ and $D_D < 0.05$ and $D_J < 0.125$. The orbit classification method identified 50 (15.1%) delta-Normids that were missed by the radiant identification method, 25 of these were recorded before or after the activity period used in the radiant method. The radiant method measured a small dispersion on the radiant with 0.66° and a radius of 1.4° was used to define the radiant size which is a compact radiant. For so many meteors with these narrow radiant criteria to fail to fit the D-criteria thresholds could indicate that these thresholds were too strict. However, statistically both selections are representative for the shower and the derived orbital parameters are in very good agreement (*Table 2*).

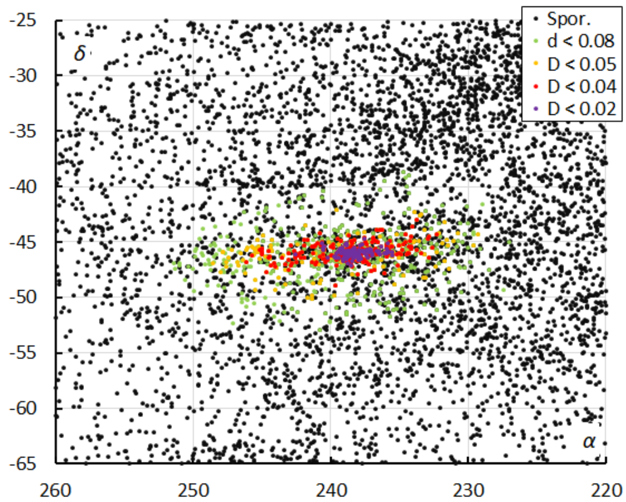

Figure 8 – The radiant distribution during the solar-longitude interval 327° – 339° in equatorial coordinates, color-coded for different threshold values of the combined similarity criteria. Spor. = sporadics.

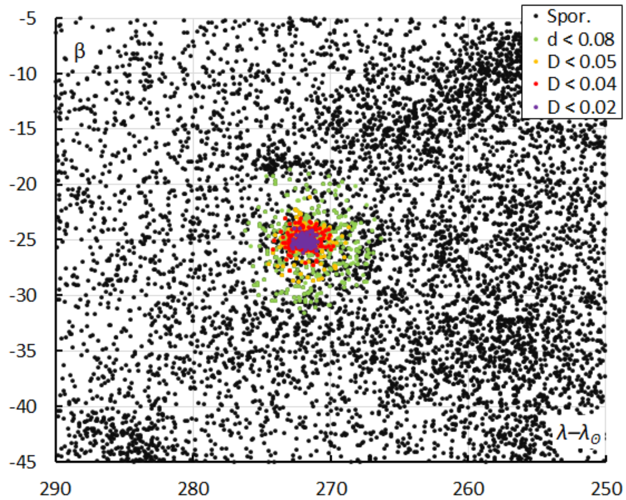

Figure 9 – The radiant distribution during the solar-longitude interval 327° – 339° in Sun-centered geocentric ecliptic coordinates, color-coded for different threshold values of the combined similarity criteria.

For the graph with the ratio delta-Normids/total-activity, only observations south of 30° in latitude were counted and the 2026 data has been processed separately from the 2020–2025 activity (*Figure 10*). The annual activity 2020–2025 barely reaches 2% of the total meteor activity with a first maximum between solar longitude 334° and 335°, and a second maximum around $\lambda_{\odot} = 339°$. In 2026 a sharp outburst occurred at the first maximum, at $\lambda_{\odot} = 334.7°$. No delta-Normids activity was detected before $\lambda_{\odot} = 326.4°$ and nothing after $\lambda_{\odot} = 344.1°$. The extended activity to

$\lambda_{\odot} = 360°$ given by Jenniskens (2023) was unable to be confirmed.

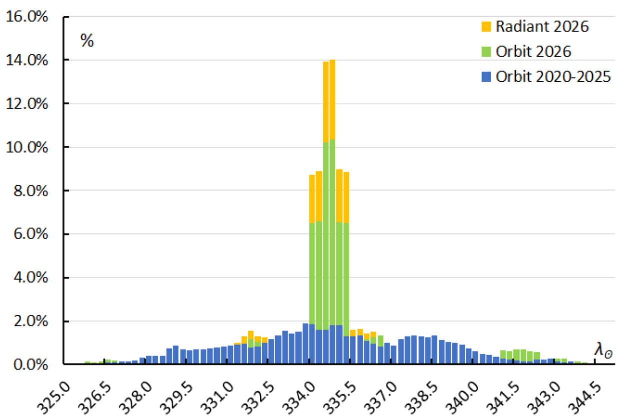

Figure 10 – The percentage of delta-Normids relative to the total number of meteors, for the radiant method (2026, orange) and the orbit classification method 2020–2025 (blue) and 2026 (green).

The profile in *Figure 10* gives the ratios counted per 1.5° (~36 hours) in solar longitude in steps of 0.25° (~6 hours). The large interval of 1.5° smooths fluctuations in the activity caused by unequal coverage at the southern hemisphere. Any sharp, sort duration peak is flattened in this graph. Compared to previous years, the delta-Normids produced an exceptional strong activity in 2026 (*Table 1*) when most meteors appeared in a short interval.

The main peak lasted about 45 minutes, with the majority of meteors appearing within 10 mins. Using 30 minutes time bins, the ZHR was around 70. It's hard to tell what the peak ZHR was during that short period as the time-area product was small, but it could have easily been greater than 100 during those 10 minutes. The meteor flux has been plotted based upon 30 minutes time bins (Vida et al., 2022). The result is shown in *Figure 11*.

Such short duration outbursts can be easily missed and this may explain why no earlier delta-Normid outbursts are know from the past. Daylight time or cloudy weather may have interfered in past years. The peak activity in 2026 was recorded by New Zealand and Australia based cameras where GMN has an excellent coverage. Future observations may reveal if the delta-Normids are an episodic shower and if the shower brings more surprises.

Table 1 – Number of delta-Normids orbits detected by GMN per year.

Year	Orbit method	Radiant method
2020	1	–
2021	2	
2022	2	–
2023	27	–
2024	48	–
2025	116	–
2026	241	281

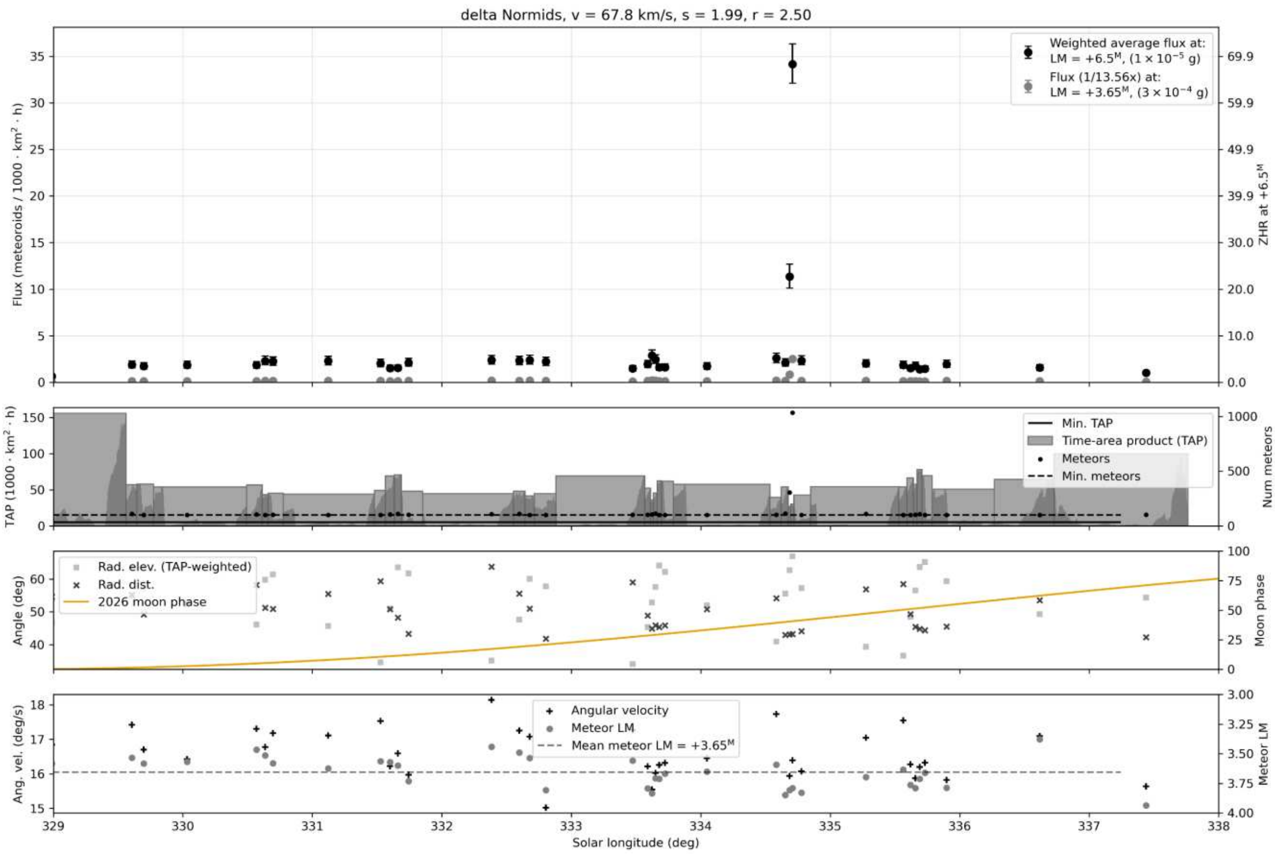

Figure 11 – The meteor flux and Zenithal Hourly Rate (ZHR) for the delta-Normids in 2026.

4 Orbit and parent body

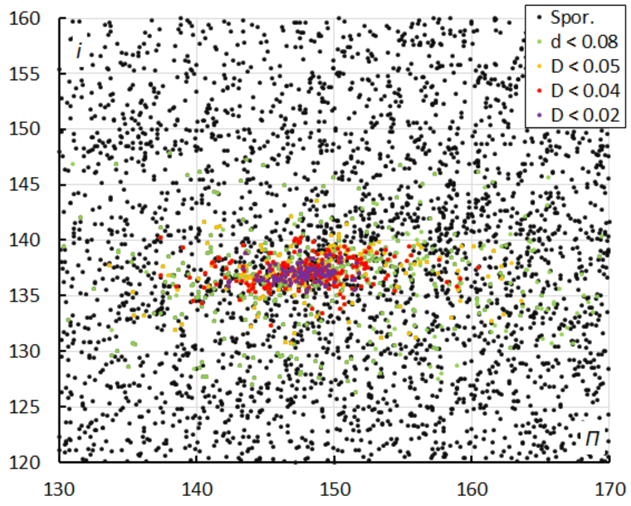

Figure 12 – Inclination i versus the Longitude of Perihelion Π color-coded for different classes of D-criteria thresholds, for $\lambda_\odot$ between 327° and 339°. Spor. = sporadics.

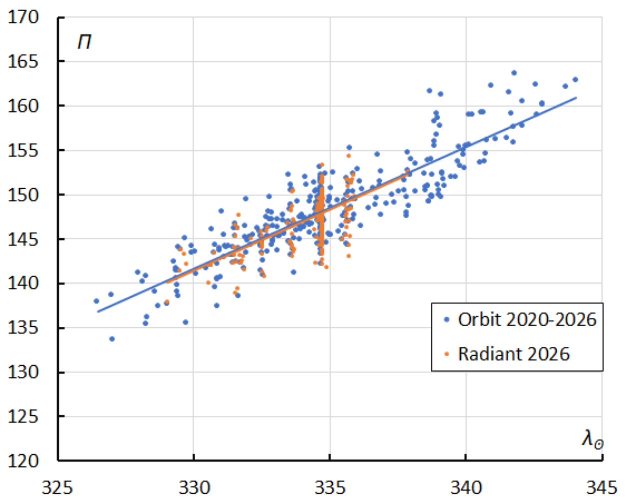

Figure 13 – The evolution of the Longitude of Perihelion Π in function of the Solar Longitude $\lambda_\odot$ based upon the radiant method (2026) and upon the orbit method (2020–2026).

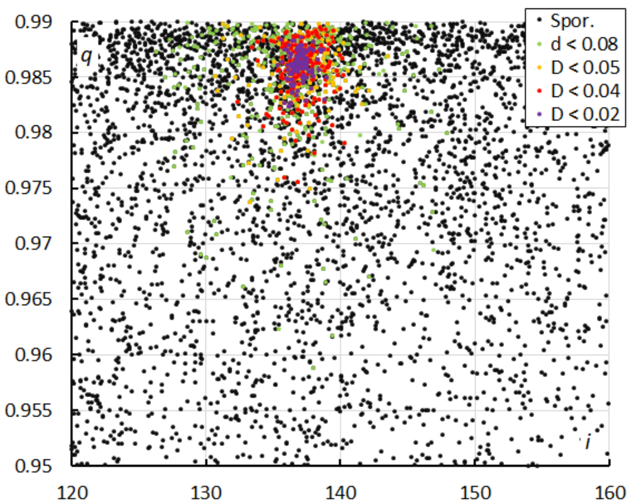

Figure 14 – Perihelion distance q versus the inclination i color-coded for different classes of D-criteria thresholds, for $\lambda_\odot$ between 327° and 339°. Spor. = sporadics.

The diagram of the inclination i versus the Longitude of Perihelion Π shows a concentration in i, stretched in Π (*Figure 12*). The spread in Longitude of Perihelion is caused by a steep increase in Longitude of Perihelion during the activity period:

$$\Pi = 1.36(\lambda_\odot - 334.7) + 148.13$$

Both methods confirm this trend (*Figure 13*). The other Kepler elements remain stable during the activity period. The cluster of DNO orbits is best visible in the diagram perihelion distance versus inclination (*Figure 14*).

Table 2 – A comparison of solutions obtained by the radiant method for 2026, the orbit method for 2020–2026 and $D_D < 0.05$ and the solution by Jenniskens (2023).

	Radiant 2026	Orbit $D_D < 0.05$	Jenniskens (2023)
$\lambda_\odot$ (°)	334.7	334.7	338.7
$\lambda_{\odot b}$ (°)	329.0	326.4	324
$\lambda_{\odot e}$ (°)	337.9	344.1	356
α_g (°)	238.5	238.5	245.5
δ_g (°)	–46.0	–46.0	–46.1
$\Delta\alpha_g$ (°)	+1.12	+1.12	+1.26
$\Delta\delta_g$ (°)	–0.14	–0.13	–0.04
v_g (km/s)	66.7	67.0	67.5
H_b (km)	113.6	114.0	114.1
H_e (km)	97.7	98.3	99.1
H_p (km)	103.6	104.0	104.4
Mag_{Ap}	–1.8	–1.6	+1.5
λ_g (°)	246.4	246.4	250.5
$\lambda_g - \lambda_\odot$ (°)	271.9	271.9	271.8
β_g (°)	–25.1	–25.1	–24.5
a (A.U.)	12.4	17.1	35.7
q (A.U.)	0.985	0.985	0.987
e	0.921	0.942	0.972
i (°)	136.9	137.1	138.3
ω (°)	353.1	353.4	353.7
Ω (°)	154.3	154.8	158.7
Π (°)	147.4	148.2	152.7
T_j	–0.46	–0.58	–0.78
N	281	437	354

The Tisserand value relative to Jupiter with $T_J = -0.46$ is typical for a long-period cometary orbit. The meteoroid stream crosses the ecliptic and Earth's orbit on a retrograde orbit ($i > 90°$) at its ascending node (*Figure 16*). The descending node crosses the ecliptic near the orbit of Neptune (*Figure 15*). A search for a possible parent body did not result in a solid match but comet C/1861 Y1 (Tuttle) could be a plausible candidate. The Drummond criterion with $D_D = 0.13$ is too weak (*Table 3*) but this may be due to this being a poorly observed comet on a parabolic orbit. The most striking resemblance is the retrograde orbit with $i = 138°$. The perihelion distance at 0.839AU, the node at 147.04° and even the eccentricity with $e = 1$ do not differ too much from the delta-Normids orbit. The largest discrepancy is in the Longitude of Perihelion with $\Pi = 118.6°$ for the comet against 147.4° for the shower. Perhaps this is related to the steep increase in Π during the shower activity period?

Table 3 – Top ten matches of a search for possible parent bodies with $D_D < 0.3$, based upon the mean orbit derived from the radiant classification method.

Name	D_D
C/1861 Y1 (Tuttle)	0.130
C/1940 S1 (Okabayasi-Honda)	0.157
C/1893 U1 (Brooks)	0.197
C/2018 Y1 (Iwamoto)	0.199
C/2015 X8 (NEOWISE)	0.201
C/1926 B1 (Blathwayt)	0.209
C/1718 B1	0.211
C/2023 X1 (Leonard)	0.24
C/1340 F1	0.242
C/1760 A1 (Great comet)	0.254

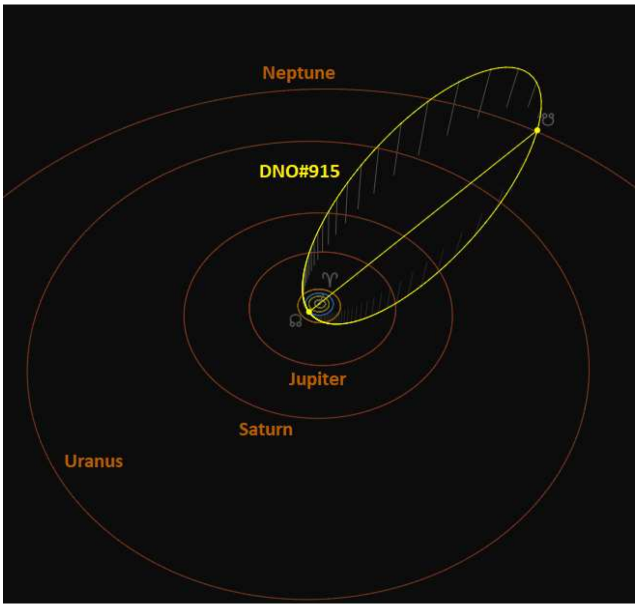

Figure 15 – The orbit determined delta-Normids solution (yellow) in the Solar System. (Plotted with the Orbit visualization app provided by Pető Zsolt).

5 Conclusion

The 2026 outburst of the delta-Normids allowed a detailed analysis of this shower and confirms the discover made by the CAMS network in 2023. Comet C/1861 Y1 (Tuttle) may be the parent body. The maximum activity level in 2026 occurred during a short time interval of 10 minutes. Based upon 30 minutes time bin the maximum ZHR was about 70. Our independent solution has been reported to the IAU-MDC, and the shower now fulfils the criteria for being nominated for established status.

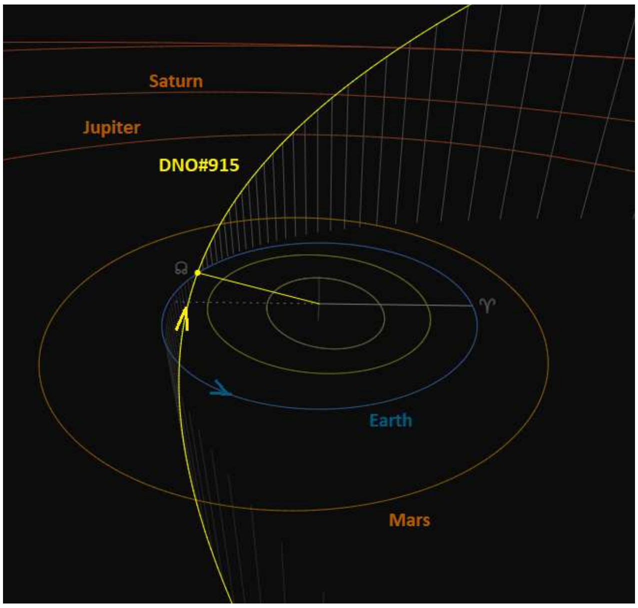

Figure 16 – The orbit determined delta-Normids solution (yellow) in the inner Solar System. (Plotted with the Orbit visualization app provided by Pető Zsolt).

Acknowledgments

This report is based on the data of the Global Meteor Network (Vida et al., 2020a; 2020b; 2021) which is released under the CC BY 4.0 license[22]. We thank all 927 participants in the Global Meteor Network project for their contribution and perseverance. A list with the names of the volunteers who contribute to GMN has been published in the 2025 annual report (Roggemans et al., 2026b). The following 353 cameras contributed to paired meteors used in this study: AU0002, AU0003, AU0004, AU0006, AU0007, AU0009, AU000A, AU000B, AU000C, AU000D, AU000E, AU000F, AU000G, AU000L, AU000Q, AU000R, AU000S, AU000U, AU000V, AU000W, AU000X, AU000Y, AU000Z, AU0010, AU0011, AU001A, AU001B, AU001C, AU001D, AU001E, AU001F, AU001K, AU001L, AU001N, AU001P, AU001Q, AU001R, AU001S, AU001T, AU001U, AU001V, AU001W, AU001X, AU001Y, AU001Z, AU0028, AU0029, AU002A, AU002B, AU002C, AU002E, AU002F, AU0030, AU0034, AU0038, AU003E, AU003G, AU003J, AU0042, AU0044, AU0045, AU0047, AU0048, AU004B, AU004K, AU004L, AU004M, AU004Q, BR000A, BR000G, BR000Q, BR000S, BR001F, BR001M, BR001R, BR001T, BR001U, BR001W, BR0029, BR002A, ES0002, ES0003, GR0006, GR0009, KR0002, KR0008, KR000A, KR000B, KR000C, KR000K, KR000L, KR0015, KR001A, KR001D, KR0024, KR0029, KR002E, KR002G, KR002K, KR002P, KR002Q, KR003Q, MX0001, MX0003, MX0007, MX0009, MX000F, NZ0003, NZ0004, NZ0007, NZ0008, NZ0009, NZ000A, NZ000B, NZ000C, NZ000D, NZ000G, NZ000H, NZ000L, NZ000M, NZ000N, NZ000P, NZ000Q, NZ000R, NZ000S, NZ000T, NZ000U, NZ000V, NZ000W, NZ000X, NZ000Y, NZ000Z, NZ0010, NZ0011, NZ0012, NZ0013, NZ0014, NZ0015, NZ0016, NZ0017, NZ0018, NZ0019, NZ001A, NZ001C, NZ001E, NZ001G, NZ001H,

[22] https://creativecommons.org/licenses/by/4.0/

NZ001J, NZ001K, NZ001L, NZ001N, NZ001P, NZ001Q, NZ001R, NZ001S, NZ001V, NZ001W, NZ001X, NZ001Y, NZ001Z, NZ0020, NZ0021, NZ0022, NZ0023, NZ0024, NZ0025, NZ0026, NZ0027, NZ0028, NZ0029, NZ002B, NZ002C, NZ002D, NZ002E, NZ002F, NZ002G, NZ002H, NZ002J, NZ002K, NZ002L, NZ002M, NZ002N, NZ002P, NZ002Q, NZ002R, NZ002S, NZ002T, NZ002U, NZ002V, NZ002W, NZ002X, NZ002Y, NZ002Z, NZ0030, NZ0032, NZ0033, NZ0034, NZ0035, NZ0036, NZ0037, NZ0038, NZ0039, NZ003A, NZ003B, NZ003C, NZ003E, NZ003G, NZ003H, NZ003K, NZ003L, NZ003M, NZ003N, NZ003Q, NZ003R, NZ003S, NZ003T, NZ003U, NZ003V, NZ003W, NZ003X, NZ003Y, NZ003Z, NZ0040, NZ0041, NZ0042, NZ0043, NZ0044, NZ0045, NZ0046, NZ0049, NZ004A, NZ004B, NZ004C, NZ004D, NZ004E, NZ004F, NZ004H, NZ004J, NZ004L, NZ004M, NZ004N, NZ004R, NZ004S, NZ004T, NZ004U, NZ004W, NZ004X, NZ004Y, NZ004Z, NZ0051, NZ0059, NZ005A, NZ005B, NZ005C, NZ005D, NZ005F, NZ005G, NZ005H, NZ005J, NZ005K, NZ005L, NZ005M, NZ005N, NZ005Q, NZ005S, NZ005T, NZ005U, NZ005Y, NZ005Z, NZ0061, NZ0063, NZ0065, NZ0066, NZ0067, NZ0068, NZ0069, NZ006A, NZ006B, NZ006C, NZ006E, NZ006F, NZ006G, NZ006H, NZ006J, NZ006K, NZ007C, NZ007E, US0002, US0003, US0004, US0005, US0007, US0008, US0009, US000A, US000C, US000E, US000G, US000J, US000K, US000L, US000M, US000R, US000S, US000V, US001E, US001Q, US001R, US0022, US0027, US002Y, US0035, US003M, US003P, US003R, US004C, US005A, US005B, US005C, US005Q, US005X, US005Y, US0062, USL003, USL004, USL005, USL00A, USL00C, USL00F, USL00G, USL00J, USL00L, USL00M, USL00N, USL00Q, USL00Z, USL011, USL012, USL013, USL016, USL017, USL01A, USL01B, USL01C, USL01D, USV003, ZA0001, ZA0006, ZA0007, ZA0008, ZA0009, ZA000C and ZA000F.

References

Drummond J. D. (1981). "A test of comet and meteor shower associations". *Icarus*, **45**, 545–553.

Jenniskens P. (2023). Atlas of Earth's meteor showers. Elsevier, Cambridge, United states. ISBN 978-0-443-23577-1. Page 537.

Jopek T. J. (1993). "Remarks on the meteor orbital similarity D-criterion". *Icarus*, **106**, 603–607.

Jopek T. J., Rudawska R. and Pretka-Ziomek H. (2006). "Calculation of the mean orbit of a meteoroid stream". *Monthly Notices of the Royal Astronomical Society*, **371**, 1367–1372.

Moorhead A. V., Clements T. D., Vida D. (2020). "Realistic gravitational focusing of meteoroid streams". *Monthly Notices of the Royal Astronomical Society*, **494**, 2982–2994.

Roggemans P., Vida D., Šegon D., Scott J.M. (2026a). "Meteoroid orbit shower identification". *eMetN Meteor Journal*, **11**, 189–204.

Roggemans P., Campbell-Burns P., Kalina M., McIntyre M., Scott J. M., Šegon D., Vida D. (2026b). "Global Meteor Network report 2025". *eMetN Meteor Journal*, **11**, 89–129.

Southworth R. B. and Hawkins G. S. (1963). "Statistics of meteor streams". *Smithsonian Contributions to Astrophysics*, **7**, 261–285.

Vida D., Gural P., Brown P., Campbell-Brown M., Wiegert P. (2020a). "Estimating trajectories of meteors: an observational Monte Carlo approach - I. Theory". *Monthly Notices of the Royal Astronomical Society*, **491**, 2688–2705.

Vida D., Gural P., Brown P., Campbell-Brown M., Wiegert P. (2020b). "Estimating trajectories of meteors: an observational Monte Carlo approach - II. Results". *Monthly Notices of the Royal Astronomical Society*, **491**, 3996–4011.

Vida D., Šegon D., Gural P. S., Brown P. G., McIntyre M. J. M., Dijkema T. J., Pavletić L., Kukić P., Mazur M. J., Eschman P., Roggemans P., Merlak A., Zubrović D. (2021). "The Global Meteor Network – Methodology and first results". *Monthly Notices of the Royal Astronomical Society*, **506**, 5046–5074.

Vida D., Blaauw Erskine R. C., Brown P. G., Kambulow J., Campbell-Brown M., Mazur M. J. (2022). "Computing optical meteor flux using global meteor network data". *Monthly Notices of the Royal Astronomical Society*, **515**, 2322–2339.

Vida D., Šegon D., Roggemans P., Wood J., Scott J., Cooke W.J., Vriezelaar A. (2026). "Delta Normid meteors 2026". CBET 5666, 2026 February 24, D. W. E. Green, editor.